Article

Electrochemical Investigation of C-Steel Corrosion Inhibition, In Silico, and Sulfate-Reducing Bacteria Investigations Using Pyrazole Derivatives

Mahmoud M. Shaban,* N. M. El Basiony,* A. Bahgat Radwan, Emad E. El-Katori,* Ahmed Abu-Rayyan, Nawal H. Bahtiti, and Moaz M. Abdou*

Read Online

ACCESS | Metrics & More | Article Recommendations | Supporting Information

ABSTRACT: The inhibitory impact of the two synthesized pyrazole derivatives (**3** and **4**) toward metallic and microbial corrosion was investigated. Using open circuit potential, potentiodynamic polarization, and electrochemical impedance spectroscopy, it was possible to determine their ability to prevent the corrosion of C-steel in 1 M HCl, which was significantly enhanced with increasing concentration (ex. 93%). They act as mixed-type inhibitors, according to polarization curves. The compounds under investigation were adsorbed on a C-steel surface in 1 M HCl following the Langmuir isotherm model. The double-layer capacitance was decreased, and the charge transfer resistance (R_{ct}) was raised due to the examined inhibitors' adsorption. Investigating changes in the surface morphology and confirming the corrosion inhibition mechanism are done using scanning electron microscopy. Density functional theory calculations and Monte Carlo simulations were also conducted to show the adsorption affinity of the understudied compounds over the steel substrate in neutral and protonated forms. Furthermore, the antimicrobial performance of the two synthesized pyrazoles against sulfate-reducing bacteria was evaluated, and the recorded inhibition efficiency was 100%. The current research shows important developments in producing highly effective anticorrosion and antimicrobial pyrazole derivatives.
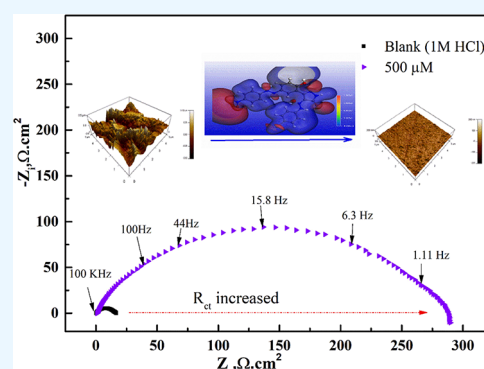
1. INTRODUCTION

Pyrazoles are widespread innovative scaffolds with a diversified land of unique properties and dual roles in inhibiting material and microbial corrosion.[1−3] C-steel is widely used in industries under various conditions. Acids are commonly used in multiple industrial processes, including oil and gas extraction and processing, pickling baths, and other chemical and petrochemical industries. Acids also appear during the technical cracking of petroleum due to the hydrolysis of salts, which may negatively impact the equipment.[4,5] Hydrochloric acid is useful in various industries, including pickling agents, etching, and cleaning. Because acids exhibit aggressive behavior, acid corrosion is critical, and the problem is costly and accounts for a significant portion of the reduction due to poor operation. Petroleum refinery units' decreased output, the price of chemicals to prevent corrosion, and high maintenance costs are drawbacks.[6,7] The majority of organic compounds with electronegative atoms (like O, S, P, and N), plane conjugated systems, and aromatic cycles (like double bonds or triple bonds) can be used as inhibitors of acid corrosion.[8−11] Adsorption of the pyrazole derivatives on the metal considerably reduces corrosion attack. As a result, it is critical to investigate the relationship between corrosion inhibition and adsorption.[12]

Given those mentioned above and in follow-up, our longstanding interest in the preparation and reactions of 1,3-diketones and their implementations,[13−22] the purpose of this study was to inspect the multidimensional insights of the synthesized pyrazoles as corrosion inhibitors and assess their inhibition efficiency on C-steel via some electrochemical measurements such as open circuit potential (OCP), potentiodynamic polarization (PP), and electrochemical impedance spectroscopy (EIS). The two synthesized pyrazoles' potential inhibitory mechanisms on C-steel corrosion were investigated using density functional theory (DFT) and Monte Carlo (MC) simulations. Furthermore, the antimicrobial activity of the two synthesized pyrazoles against sulfate-reducing bacteria (SRB) was evaluated. The most bacterially influenced corrosion is SRB, as is well known.[23,24] In the

Table 1. Comparison between Parallel Corrosion and Biocidal Activities of Recent Multifunctional Inhibitors and This Work

compounds code	corrosive medium	corrosion inhibition		SRB inhibition		ref
		optimum dose	max. inhibition %	optimum dose	max. inhibition %	
TOS3	10% HCl	50 ppm	87.6	50 ppm	80	23
MA-1156	1 M HCl	18 μM	86.4	16 μM	80	24
SPT	formation water	200 ppm	79.0	80 ppm	100	25
Pz1	5 M HCl	2000 ppm	91.0	20 ppm	83.3	26
Pz2			89.0		100	
3	1 M HCl	500 μM	93.6	30 ppm	100	our work
4			94.7		100	

literature, numerous reports demonstrate the effectiveness of corrosion inhibitors against SRB (cf. Table 1).[3,25]
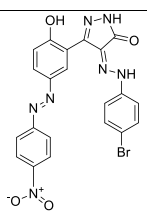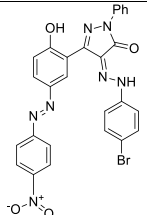
2. EXPERIMENTAL SECTION

2.1. Materials. The following C-steel specimens were used for all measurements: 0.200% C, 0.350% Mn, 0.024% P, and 0.003% S, and the remaining weight percent is Fe. The C-steel working electrode surface was glossed as a mirror finish via various grades (200−2000) from gravel emery papers, cleaned, and washed via bi-distilled water and acetone for removing greases. The concentration range of the examined inhibitors was between 1 and 500 μM.

2.2. Solutions. Hydrochloric acid (37%), acetone, and ethyl alcohol were bought from Algomhoria Company in Egypt. All measurement solutions were made with bi-distilled water.

2.3. Synthesis of the Inhibitors. Two selected azo pyrazoles, **3** and **4**, were synthesized via our previous protocol and are listed in Table 2.[26−29]

Table 2. Molecular Structure, Molecular Weight, and Molecular Formulas of the Examined Two Pyrazole Derivatives 3 and 4

compounds	structure formula	mol. weight	mol. formula
3		508.29	$C_{21}H_{14}BrN_7O_4$
4		584.39	$C_{27}H_{18}BrN_7O_4$

2.4. Electrochemical Measurements. An ordinary three-compartment glass cell was used for the electrochemical measurements. The working electrode was a C-steel (1 cm^2), the reference electrode was a saturated calomel electrode (SCE), and the counter electrode was a platinum sheet (1 cm^2). To reduce IR drop, the working electrode's surface was made to touch the tip of a Luggin capillary attached to the reference electrode. All measurements were conducted without stirring in solutions exposed to the atmosphere. All potential data were reported in comparison to SCE. The electrode was prepared for each experiment by abrading it with progressively finer emery paper, degreasing it with acetone, washing it with bi-distilled water, and drying it. To generate Tafel polarization curves, the electrode potential was automatically changed from (−0.8 to −0.2 V vs SCE) at open circuit potential with a scan rate of 1 mV s^{-1}. The Stern−Geary method, which measures corrosion current, extrapolates the anodic and cathodic Tafel lines of charge transfer-controlled corrosion reactions to the point that yields (I_{corr}) and the corresponding corrosion potential (E_{corr}) in the absence and presence of the examined inhibitors. Then, the following formulas were used to calculate the inhibitory efficiency (IE %) and surface coverage (θ):

$$IE\% = \theta x \, 100 = (I_{corr.free} - I_{corr.inh})/I_{corr.free} \qquad (1)$$

$I_{corr.free}$ and $I_{corr.inh}$ are the corrosion current densities in the absence and presence of an inhibitor, respectively.

Impedance measurements were taken using AC signals at OCP in a frequency range of 100 kHz to 0.1 Hz and an amplitude of 5 mV peak-to-peak. The parallel circuit was used to examine and interpret the experimental impedance. The major parameters determined from the Nyquist curve investigation are the double-layer C_{dl} capacity and the resistance of charge transfer R_{ct} (the high-frequency loop diameter). The following relationships describe the inhibition efficiency (IE %) and surface coverage (θ) determined from impedance measurements:

$$IE\% = \theta x 100 = (R_{ct.inh} - R_{ct.free})/R_{ct.inh} \qquad (2)$$

$R_{ct.free}$ and $R_{ct.inh}$ are the charge transfer resistance in the absence and presence of an inhibitor, respectively.

Before the measurements, the electrode potential was allowed to settle for 30 min. All investigations were carried out at a temperature of 25 ± 1 °C. The measurements were made with a Versa STAT 4 potentiostat/galvanostat coupled to a laptop "All in one" and a frequency response analyzer (FRA). The electrochemical test methods were performed following the guidelines of ASTM G59-97, ASTM G102-89, and ASTM G3-89.

2.5. Theoretical Quantum Chemical Study. Materials Studio (6.0) software executes the quantum calculation study for the prepared **3** and **4** pyrazole compounds in neutral and protonated forms. The GGA approach with DNP-3.5 bases set included in the DMol3 module was selected for the geometry optimization process. The energy values of frontier molecular orbitals (FMOs) of pyrazole derivatives (E_H, and E_L) are extracted after the geometry optimization process. The energy difference (ΔE_{gap}) between FMOs is the function of pyrazole derivative compounds **3** and **4** reactivity. The MC simulation process is conducted in gas and simulated acidic solution to

mimic the real corrosion environment of the steel alloy. MC was run with an adsorption locator module implemented in the MS (6.0) software. Fe (1 1 0) is selected due to its stability. The iron crystal with cleavage (1 1 0) is imported and extended to the (15 × 15) supercell, and the vacuum slap with thickness 15 A° created over the iron crystal plane. The COMPASS force field controlled the annealing process, as previously described.[30] MCs run via 10,500 steps to attain the equilibrium configuration of the system.

2.6. Surface Analysis. Measurements of surface topography and roughness of the C-steel were performed employing an Asylum Research MFP-3D atomic force microscope, AFM (Santa Barbara, CA, USA). The surface roughness has been detected for the polished C-steel coupon and those immersed for 6 h in pure 1 M HCl and treated with 500 μM of the best corrosion inhibitor 4.

2.7. Microbial-Induced Corrosion (MIC). As a result of the favorable anaerobic conditions it offers for the growth of bacteria like SRB, the produced oil tanks' lowest level can be regarded as a significant MIC source. In such vulnerable locations, MIC attacks caused by SRB can lead to catastrophic consequences. The Egyptian Petroleum Research Institute (EPRI) made particular growing medium kits available. To replicate the anaerobic conditions described in NACE TM0194/14 86, such media were created and contained in separate vials. The NACE TM0194/14 and our prior study were used as the basis for the standard sample process and data gathering.[1−3]

3. RESULTS AND DISCUSSION

3.1. Synthesis of the Inhibitors 3 and 4. As we previously reported,[26−29] the synthetic approach for preparing bis-azo pyrazoles 3,4 is depicted in Scheme 1. Diazo coupling of azo pyrazoles 1,2 with 4-nitrophenyl diazonium chloride in a basic solution yielded pyrazoles 3,4.

Scheme 1. Synthesis of Bis-azo Pyrazoles 3,4
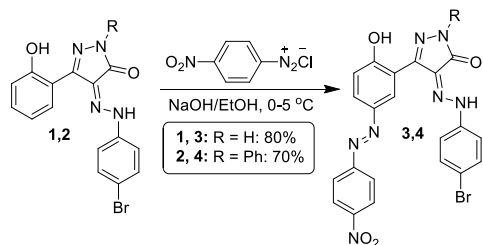
3.2. Electrochemical Measurements. *3.2.1. Open Circuit Potential.* Figure S1 shows the OCP variation over time for the inhibitor chemical 4 with a 30-minute immersion duration. After a sharp increase in the negative direction of the potential, the OCP plots reached a steady state area, which suggests that an equilibrium state between the oxidation and reduction processes with a zero-bias potential was achieved at all concentrations of the added inhibitor compound 4 series.[3] Regarding the direction of the OCP or the values of the E_{OCP}, the behavior of the blank sample and the other inhibited samples was essentially the same. As a result, the compound 4 series molecules can be referred to as mixed-type inhibitors since they can stifle both cathodic and anodic processes.

3.2.2. PP Measurements. Figure 1 displays the anodic and cathodic Tafel polarization curves for C-steel in 1 M HCl in

the absence and presence of different concentrations of the examined inhibitors (3 and 4) from 1 to 500 μM at 25 °C. It is clear from Figure 1 that the two synthetic pyrazole inhibitors under investigation work to delay the anodic dissolving of C-steel and the cathodic hydrogen discharge processes in 1 M HCl and that this inhibition became more pronounced when the inhibitors' concentrations were raised. Table 3 lists the electrochemical parameters that were determined using Tafel curves, including corrosion current density (I_{corr}), E_{corr}, Tafel slopes (β_a and β_c), inhibition efficiency (IE %), and degree of surface covering (θ). Raising the concentration of the synthetic inhibitors, Tafel lines are moved to more negative and positive potentials when the blank curve is considered. This behavior is normally estimated because of the inhibitor's (mixed-nature inhibitor) adsorption onto the C-steel surface, which inhibits both the cathodic and anodic processes.[31] The change in the corrosion potential in ±85 mV around the E_{corr} of C-steel in a blank solution confirmed the mixed adsorption nature of compounds 3 and 4. According to the results, an increase in inhibitor concentrations causes a decrease in I_{corr} due to the presence of electron-donating groups (aromatic and hetero-aromatic rings (pyrazolone, phenylhydrzenylidene, and phenyl-pyrazolone) and halide and nitro) that help the tested compound adsorption on the C-steel surface. Still, the Tafel slopes (β_a and β_c) are roughly constant, showing that the two reactions (anodic metal dissolution and cathodic hydrogen reduction) were delayed without the dissolution mechanism changing.[32] According to the Stern−Geary equation, the polarization resistance (R_p) of the X-65 steel value is a reciprocal function of I_{corr}.

$$R_p = \frac{y}{I_{corr}} \tag{3}$$

where y is constant and equal to $\left[(\beta_a \beta_c)/2.303(\beta_a + \beta_c) \right]$. Due to their blocking active center effect, the adsorption of pyrazole derivatives increases the polarization resistance via the retardation ionization or dissociation of metal.[3] As the molecular weight of the inhibitor molecule increases, its inhibition performance increases. Thus, the inhibition efficiency of compound 4 > compound 3.

3.2.2.1. Effect of Temperature. The temperature enhances the offensive effect of HCl on the corrosion reaction of C-steel. The temperature boosted the kinetic motion of the HCl solution, which leads to decreasing both the corrosion products deposited and the protective film on the metallic surface, which increases iron ionization and hydrogen gas evolution. PP measurements were used to investigate the impact of temperature on the C-steel corrosion rate in 1 M HCl with 500 μM of the examined inhibitors at temperatures between 298 and 318 K (Figure S3). Table 4 lists the effects of temperature on the effectiveness of the inhibition for C-steel in 1 M HCl when the examined inhibitors are present and absent. According to the results, raising the temperature rapidly impacts the corrosion rate in the absence and presence of 500 μM of the pyrazole derivatives (3 and 4). The rising temperature increased the corrosion current density of C-steel from 0.95 and 0.0502 to 1.856 and 0.360 mA cm^{-2} in the absence and after the addition of 500 μM of compound 4, respectively (Table 4). The adsorption film of 500 μM of compound 4 over the C-steel enhanced its activation energy calculated from eq 4 and slope of Figure 2 to 82.9 kJ mol^{-1} as reported in Table 5. This finding implies that the examined
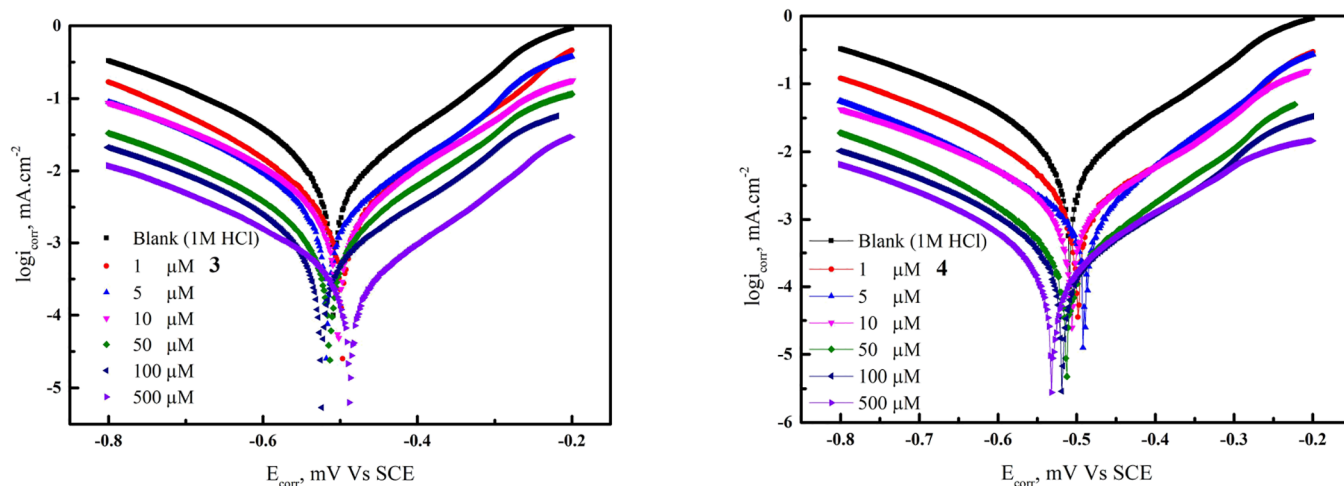
Figure 1. Potentiodynamic polarization curves for C-steel corrosion in 1 M HCl in the absence and presence of various concentrations of compounds **3** and **4** at 25 °C.

Table 3. Electrochemical Kinetic Parameters of the Tafel Curves for C-Steel Immersed in 1 M HCl without and with Various Doses of the Examined Inhibitors

inhibitors	conc., (μM)	$-E_{corr.}$ mV (vs SCE)	$I_{corr,}$ μA cm^{-2}	β_a, mV dec^{-1}	$-\beta_c$, mV dec^{-1}	R_p $\Omega\cdot$cm^2	θ	IE %
blank		509.2 ± 3.7	950.2 ± 1.12	110.5 ± 3.15	136.4 ± 3.35	27.90		
3	1	497.1 ± 5.7	420.25 ± 3.35	101.3 ± 3.58	125.65 ± 4.12	57.95	0.5577	55.77 ± 3.51
	5	518.4 ± 5.3	298.1 ± 3.52	106.1 ± 3.42	128.5 ± 3.68	84.65	0.6862	68.62 ± 3.18
	10	502.5 ± 3.3	189.5 ± 3.81	85.74 ± 2.78	130.15 ± 1.18	118.56	0.8005	80.05 ± 2.80
	50	513.7 ± 3.6	100.5 ± 4.01	84.53 ± 1.68	132.15 ± 5.21	222.74	0.8942	89.42 ± 3.78
	100	523.2 ± 5.9	82.7 ± 2.05	78.5 ± 2.91	127.8 ± 4.36	255.33	0.9129	91.29 ± 2.27
	500	489.3 ± 5.1	60.21 ± 2.85	82.5 ± 2.25	130.1 ± 3.44	364.09	0.9366	93.66 ± 2.65
4	1	498.6 ± 2.3	361.52 ± 5.32	105.6 ± 5.24	128.5 ± 3.58	69.62	0.6195	61.95 ± 2.96
	5	492.7 ± 2.7	240.1 ± 2.75	101.1 ± 3.05	125.4 ± 4.42	101.23	0.7473	74.73 ± 1.58
	10	506.4 ± 4.8	153.2 ± 3.42	105.5 ± 3.48	127.6 ± 4.48	163.68	0.8387	83.87 ± 1.47
	50	512.7 ± 5.8	95.61 ± 4.38	82.5 ± 1.63	125.4 ± 3.02	226.0	0.8993	89.93 ± 1.94
	100	519.3 ± 3.1	72.5 ± 2.68	80.1 ± 1.87	123.6 ± 3.37	234.51	0.9239	92.39 ± 2.08
	500	531.5 ± 5.4	50.2 ± 1.21	75.2 ± 1.78	124.9 ± 2.29	295.4	0.9471	94.71 ± 0.71

Table 4. Effect of Temperature on the C-Steel Corrosion in 1 M HCl in the Absence and Presence of 500 μM of Tested Inhibitors

		298 K		308 K		318 K	
	conc (μM)	I_{corr}, μA/cm^2	IE, %	I_{corr}, μA/cm^2	IE, %	I_{corr}, μA/cm^2	IE, %
blank	0.00	950.2		1254.1		1856.2	
3	500	60.21	93.66	204.3	83.70	470	74.67
4	500	50.2	94.71	160.4	87.21	360.5	80.57

inhibitors' ability to prevent corrosion is possibly due to the higher energy barrier for metal breakdown.[33]

$$\ln I_{corr} = \ln A - \left(\frac{E_a}{RT}\right) \quad (4)$$

where A and R are the Arrhenius and gas constant, respectively.

3.3. EIS Measurements. Impedance measurements give information on the interface's resistive and capacitive behavior, as well as an assessment of the effectiveness of the examined compounds as potential corrosion inhibitors and an investigation of the mechanisms underlying corrosion inhibition. Using EIS, further details on the corrosion behavior of C-steel in 1 M HCl with and without the tested pyrazole inhibitors may be obtained. This clarifies that the presence of pyrazole derivatives increases the diameter of the capacitive loops without altering

their shapes.[34] This behavior indicates an inhibitive film that impedes C-steel corrosion in HCl. The following equation is used to get the double-layer capacitance (C_{dl}) and the frequency at which the imaginary part of the impedance is at its maximum ($-Z_{max}$):

$$C_{dl} = \left(\frac{1}{2\pi f_{max} R_{ct}}\right) \quad (5)$$

where f_{max} is the maximum frequency at which the imaginary component of the impedance (Z_{imag}) is maximum and R_{ct} is the diameter of the loop.

Figure 3 demonstrates that adding the examined compound **4** increases R_{ct} values, reaching 94.29% at 500 μM without altering the impedance shape. The Nyquist plots in Figure 3 did not form perfect semicircles as predicted by the EIS theory,
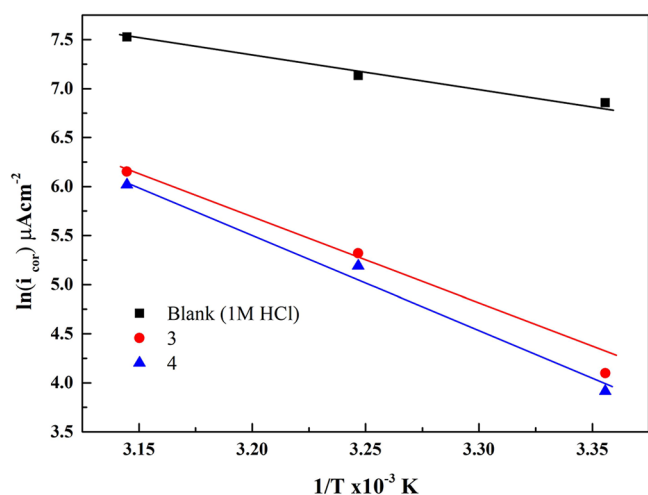
Figure 2. Arrhenius relation for C-steel in 1 M HCl in the absence and presence of 500 μM of pyrazole derivatives (**3** and **4**) at different temperatures.

Table 5. Thermodynamic Activation Data for C-Steel Corrosion in 1 M HCl in the Absence and Presence of 500 μM 3 and 4 Inhibitors

solution	E_a (kJ mol^{-1})
blank	26.32
3	81.08
4	82.95

showing a general behavior where the double layer on the metal/solution interface does not act as a real capacitor. The findings in Table 6 demonstrated that as the concentration of inhibitors rose, R_{ct} values increased, and the capacitance, C_{dl}, values dropped. The reduction in capacitance showed that the inhibitor molecules adsorbed at the metal/solution interface. This may happen when the local dielectric constant decreases, or the electrical double-layer thickness rises. A lower C_{dl} value was obtained when the inhibitors were added, possibly due to inhibitor molecules replacing water molecules at the C-steel electrode surface. The inhibitor compounds may also lower capacitance by thickening the double layer.[35] Exploring the data reveals that each impedance diagram in Figure S2 Bode-phase plots comprises a sizable capacitive loop with a single capacitive time constant. Higher concentrations cause the

capacitance loop's diameter to increase, which indicates how much the corrosion process is inhibited. The modulus impedance $|Z_{mod}|$ and phase angle degree values, respectively, at lower and intermediate frequency regions, have been enhanced by adding pyrazole derivatives (**3** and **4**). This also confirmed the inhibitory effects of the understudied compounds. The general explanation for this inductive loop is the adsorption of species brought on by the dissolution of C-steel and hydrogen adsorption. Finally, the bigger Z_{mod} indicates stronger inhibitor protection for C-steel.[36]

The electrical circuit depicted in Figure 4 that was used to simulate the gained EIS data has three components: R_{ct}, C_{dl}, a double-layer capacitance, and R_s, which stands for the solution resistance.

3.4. Adsorption Isotherm. The adsorption isotherm that characterizes the metal/inhibitor/environment system may be derived, which is one of the most suitable methods for quantitatively describing adsorption.[37] In 1 M HCl solution, the examined inhibitors were diluted to various concentrations, and the degree of surface covering (θ) values were calculated. Various electrochemical experiments were used to quantify the extent of surface covering (θ). Different adsorption isotherm models were fitted using surface coverage (θ) data, and the correlation coefficient (R^2) was used to choose the best isotherm, which was found to follow the Langmuir adsorption isotherm and expressed by:[38]

$$C/\theta = \left(\frac{1}{K_{ads}}\right) + C \tag{6}$$

C_{inh} is the inhibitor concentration, and K_{ads} is the adsorption equilibrium constant. The drawing of (C/θ) vs (C) for concentrations of the examined inhibitors is illustrated in Figure 5. It was discovered that the studied inhibitors had a straight-line association. The equilibrium constant (K_{ads}) values are recorded in Table 7. The higher values of (K_{ads}) of the examined inhibitors the higher the adsorption of the tested inhibitors on the surface of C-steel immersed in 1 M HCl. The following relationship exists between the free energy of adsorption, $\Delta G°_{ads}$, and the equilibrium constant of adsorption (K_{ads}), which is determined by the slope of the Langmuir adsorption isotherm:[39−41]

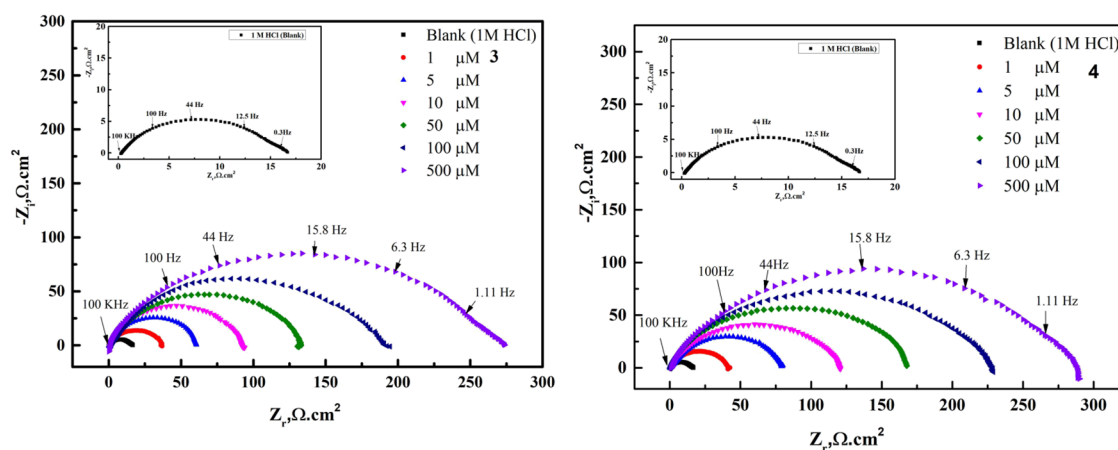$$\Delta G°_{ads} = -RT\ln(55.5\,K_{ads}) \tag{7}$$

Figure 3. Nyquist fitted curves recorded for C-steel in 1 M HCl with and without various compound **3** and **4** concentrations at 25 °C.

Table 6. Electrochemical Parameters Obtained from EIS Equivalent Circuit Fitting of C-Steel Immersed in 1 M HCl without and with Various Doses of the Examined Inhibitors

inhibitors	conc., (μM)	R_s, (Ω cm^2)	n	C_{dl}, (μF/cm^2)	R_{ct}, (Ω cm^2)	IE %
blank		1.391	0.961	107.23 ± 2.26	16.85 ± 1.76	
3	1	1.568	0.997	57.91 ± 3.17	36.2 ± 2.47	53.45 ± 3.51
	5	1.232	0.996	52.27 ± 2.58	62.4 ± 3.47	72.99 ± 3.18
	10	1.184	0.995	49.23 ± 1.64	98.52 ± 2.59	82.89 ± 4.80
	50	1.049	0.994	43.56 ± 2.69	134.28 ± 1.43	87.45 ± 3.78
	100	1.289	0.999	30.71 ± 3.14	194.57 ± 2.27	91.33 ± 1.27
	500	2.174	0.976	18.06 ± 2.78	271.31 ± 2.37	93.78 ± 1.46
4	1	1.7025	0.996	50.84 ± 3.69	47.6 ± 1.74	64.60 ± 1.58
	5	2.260	0.993	46.19 ± 4.28	79.95 ± 2.51	78.92 ± 1.47
	10	1.607	0.998	40.65 ± 3.75	127.6 ± 2.11	86.79 ± 1.94
	50	1.367	0.996	28.37 ± 1.49	180.8 ± 3.43	90.68 ± 1.64
	100	1.409	0.984	22.13 ± 1.84	234.51 ± 2.57	92.81 ± 2.08
	500	1.375	0.99	6.39 ± 2.37	295.4 ± 1.68	94.29 ± 0.71
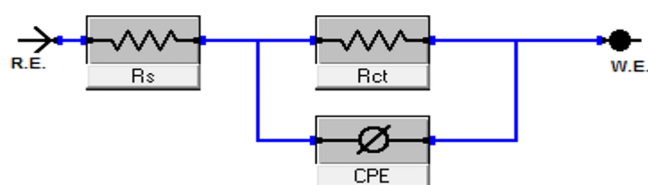
Figure 4. Parallel electrical circuit model utilized to fit EIS results.

55.5 is the molar water concentration in mol L^{-1}, R is the gas constant, and T is the absolute temperature. Data in Table 7 display values of ($\Delta G°_{ads}$); large values of ($\Delta G°_{ads}$) and their negative sign are often indicative of strong interaction and very effective adsorption.[37] Values of ($\Delta G°_{ads}$) around −40 kJ mol^{-1} are often consistent with chemisorption at room temperature.[42]

3.5. Theoretical Quantum Chemical Study. DFT has been used to give an expectation about the pyrazole derivative's chemical structures and their inhibitory activity. Optimized pyrazole derivatives structure and their FMOs in addition to the electrostatic potential mapping (ESP) shown in (Figure 6) for the neutral form and Figure S4 for the protonated form. The energies of the highest occupied molecular orbital (HOMO) (E_H) and the lowest unoccupied molecular orbital (LUMO) (E_L) exported from the Dmol3 module are used to calculate the other relevant parameters

tabulated in Table 8 according to the following eqs 8−9101112:

$$\Delta E_{gap} = E_L - E_H \tag{8}$$

$$\eta = \frac{E_L - E_H}{2} \tag{9}$$

$$E_{b \to d} = \frac{E_H - E_L}{8} \tag{10}$$

$$\chi = \frac{\Delta E_{gap}}{2} \tag{11}$$

$$\Delta N = \frac{(x_{Fe} - \chi_{compd})}{(2\eta_{compd})} \tag{12}$$

where η is the global hardness, χ, is the pyrazole derivative electronegativity, ΔN is the fraction of transferred electrons, $E_{b \to d}$ is the energy of back donation, and x_{Fe} is the electronegativity of the Fe (1 1 0) plane that is 7.[43,44]

The optimized configuration of the studied compounds is obtained through a geometry optimization process, where the force on the coordinated atoms is brought to zero. The optimized structure shows how the studied compounds are planar in different studied forms (neutral or/and protonated), which greatly subjected the active sites of these compounds to
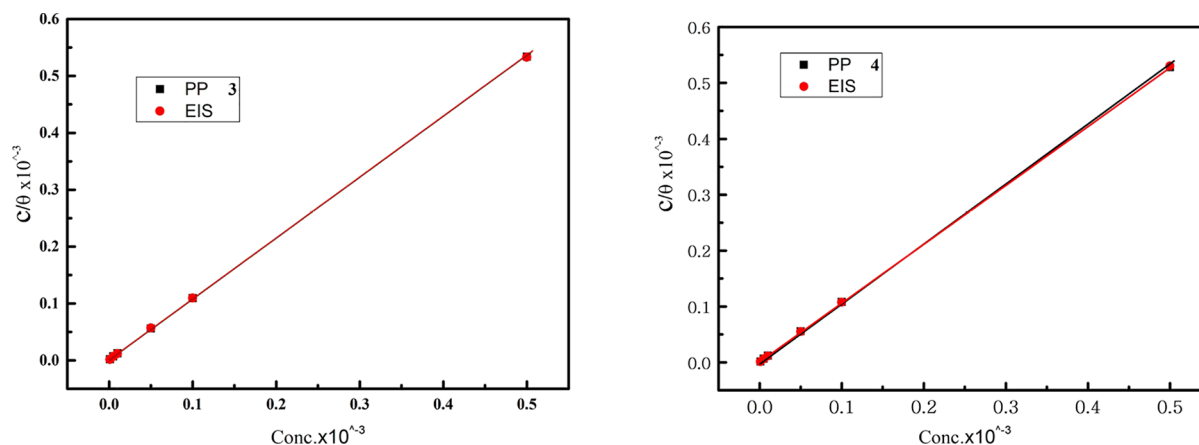
Figure 5. Langmuir adsorption isotherm for C-steel dissolution in 1 M HCl involving different concentrations of the examined compounds **3** and **4** at 25 °C.

Table 7. Langmuir Adsorption Parameters for the C-Steel Dissolution in 1 M HCl Involving Different Concentrations of the Examined Inhibitors at Room Temperature

inhibitors	experimental methods	$-\Delta G^{\circ}_{ads}$ (kJ mol^{-1})	$K \times 10^5$ (L mol^{-1})	slope	R^2
3	PP	42.4	4.96	1.064	0.9997
	EIS	42.3	4.7	1.067	0.9997
4	PP	42.7	5.59	1.037	0.9998
	EIS	43.6	7.83	1.052	0.9995
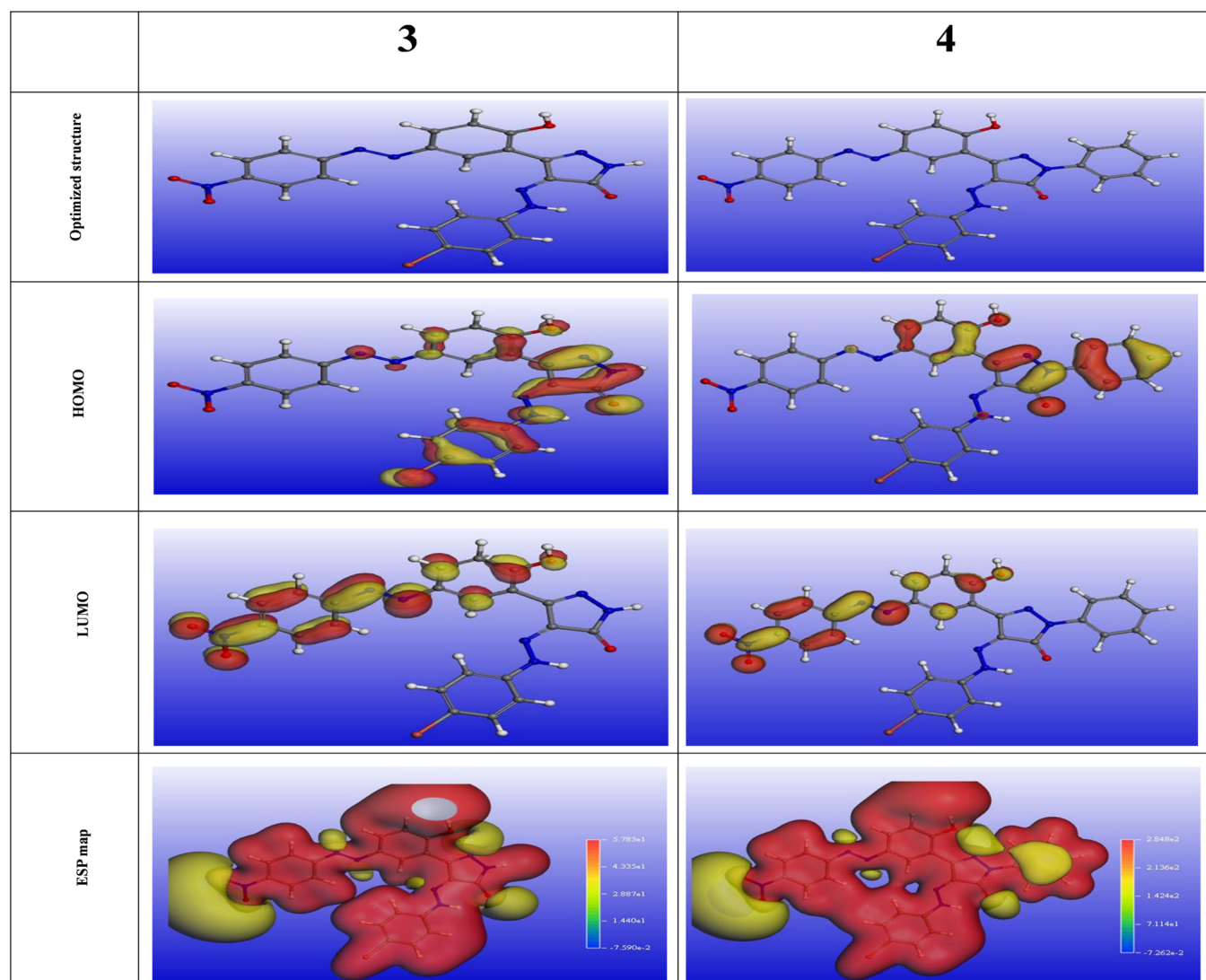
Figure 6. Optimized molecular structures with electronic densities of HOMO, LUMO, and ESP map of the examined compounds in neutral form.

Table 8. Quantum Chemical Parameters of the Examined Two Pyrazole Derivatives

quantum parameters	3	4
E_H (eV)	−5.258	−5.082
E_L (eV)	3.591−	3.615 −
ΔE (eV)	1.667	1.467
X (eV mol^{-1})	4.424	4.349
η (eV mol^{-1})	0.833	0.733
$E_{b \rightarrow d}$ (eV mol^{-1})	−0.208	0.183−
ΔN	1.993	2.043

the substrate. This indicates that these compounds are highly likely to interact with the metallic surface via planar aromatic moieties.[45] Based on Mulliken charge distribution, the higher the atomic charge value, the higher the protonation affinity. O7 of compounds **3** and **4** has the highest Mulliken atomic charges, −0.568 and −0.602. Thus, these atoms have the highest protonation affinity. The concentrated electron clouds over aromatic and hetero-aromatic rings (pyrazolone, phenyl-hydrzenylidene, and phenyl-pyrazolone) and halide and nitro groups represent the active centers that participate in the interaction between the prepared compounds and d-orbitals of iron. The higher energies of the HOMO and lower energies of the LUMO represent the higher affinity of these compounds to interact easily with the 3-d orbital of Fe. This indicates the iron corrosion suppression activity of these compounds.[46] The electron density distribution over the whole compound structure is clearly shown in ESP mapping. This confirms the

ability of these compounds to form a stable compacted layer over the iron surface and, in turn, decrease the offensive action of HCl. The energy of the HOMO indicates the ability of organic inhibitors to donate electrons to the 3d-orbital of Fe. The higher the E_H, the easier the electron donation and adsorption affinity. From Tables 8 and S1, the E_{HOMO} of compound 4 is higher than that of compound 3. This confirms the higher effective action of compound 4 over compound 3. This is matched with the experimental results.

Moreover, the E_{HOMO} values of compounds 3 and 4 in the protonated form are higher than those in the neutral form. This may indicate that the understudied compounds' protonated forms make these compounds interact strongly with the iron surface. The E_{b-d} values for the 3 and 4 compounds in neutral and protonated form indicate the affinity of the LUMO to accept electrons from the full-filled 3d-orbital of Fe.[47] This, in turn, enforces the donor-acceptor interaction between 3 and 4 compounds and Fe. Hardness (η) and softness(σ) are important parameters that help predict corrosion inhibitors' adsorption affinity. As reported, a highly reactive molecule (soft) has a lower ΔE value and vice versa for the lower reactive one (hard).[48] Compound 4 has lower η values than compound 3 in the different studied forms. The energy gap between the HOMO and LUMO indicates the easy transfer of electrons and the stable complex formed between the prepared compounds and iron. The lower the ΔE_{gap} the higher the potential corrosion inhibition. According to the data in Tables 8 and S1, compound 4 has higher efficiency as a corrosion inhibitor than compound 3, which matches the experimental data. The HOMO of 3 and 4 compounds transmits electrons to iron when the electron transfer (ΔN) fraction has positive values. The ΔN-provided values demonstrate that the examined compounds were inhibited in the order of 4>3. The whole quantum calculated parameters indicate that compound 4 in both forms (neutral and protonated) has higher interaction adsorption affinity with the Fe than compound 3.

The experimental data extracted from EIS and PP were consistent with the estimated DFT values. To simulate the corrosion inhibition process of the iron alloy and to imagine the adsorption configuration of the pyrazole derivatives compounds (3 and 4) over the iron plane surface (1 1 0), the adsorption locator module in MS.6.0 software controlled with COMPASS forcefield applied for 3&4/Fe (1 1 0) system in gas and simulated acid solution $100H_2O$ + 5HCl phases. The most stable arrangement of the examined inhibitors (3 and 4) across the Fe (110) plane is shown in Figure 7 in both the gaseous and simulated acidic solution phases. The top and side perspectives of the examined inhibitor (3 and 4) configurations provide important details that may be quickly explained as follows:

- The parallel orientation of the 3 and 4 to Fe (110) plane is displayed clearly from the side caption views.
- Top views also demonstrated the planarity of compounds 3 and 4, which occupy and cover a substantial portion of the surface of Fe (110).

The side and top views display the high adsorption affinity of the pyrazole derivatives on the steel surface, where the active centers (aromatic and hetero-aromatic rings (pyrazolone, phenylhydrzenylidene, and phenyl-pyrazolone) and halide and nitro groups) become more subjected to the steel surface. This, in turn, enhances the inhibitory effect of these
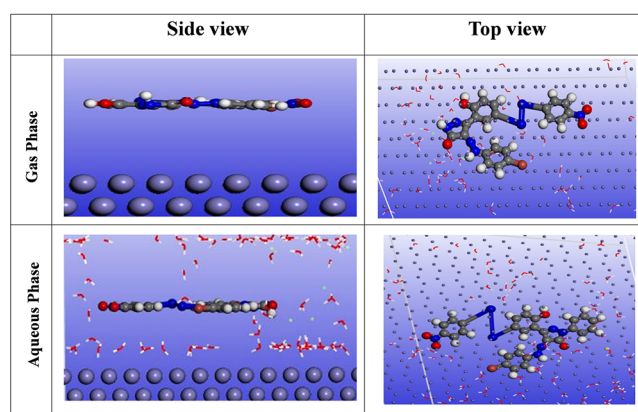
Figure 7. Side and top view snapshots of the most stable orientation of the examined compounds simulated as whole parts in different phases.

compounds.[49] The resultant adsorption energy values (E_{ads}) for compounds 3 and 4 are shown in Table 9, confirming their adsorption affinity. The stronger and more permanent the adsorption of 3 and 4 on iron, the bigger the negative value of E_{ads}. Compound 4 faces more adsorption competition from molecules of H_2O, H_3O^+, and Cl^- ions in its current state. This finding, which demonstrates the propensity of compound 4 to replace these adsorbed ions/molecules at the iron contact, is consistent with the electrochemical evidence previously discussed.[30,50]

3.6. Mechanism of Corrosion Inhibition. The inhibition efficiency of C-steel corrosion in 1 M HCl solution by the two synthesized pyrazoles (3 and 4) using the above techniques was established to depend on different factors such as the concentration of the synthesized inhibitors, the number of adsorption active centers in the inhibitor and their charge density, molecular size, and stability of this inhibitor in aggressive solutions.[51] On the metal surface, the active centers for adsorption are nitrogen and oxygen. The examined inhibitors adsorb onto the surface of the C-steel, blocking the active centers and reducing corrosion attacks. Based on the donor–acceptor interaction between the π-electrons of the donor groups of the inhibitors and the unoccupied orbitals of iron surface atoms, the adsorption of the inhibitor molecules on the surface of the C-steel may be explained.[52–55] The inhibitors containing nitrogen, oxygen, and π-bonds can provide effective inhibition, compared with inhibitors containing only one of them.[56] The adsorption is assumed mainly through the nitrogen and oxygen atoms in the examined two synthesized pyrazoles (3 and 4) (active centers).

Generally, the corroded C-steel surface in HCl solution carries −Ve charge due to the electrostatic adsorption of Cl^- ions on the steel surface $(FeCl^-)_{ads}$.

Thus, we suggest the pyrazole derivative adsorption follows one of these pathways or all of them:

one is the attraction force between the positively charged atoms (nitrogen or oxygen) and the negatively C-steel-charged centers. The other pathway is the pyrazole compounds form a complex with the Fe^{+2} ions formed over the C-steel surface. This electrostatic force enhances the pyrazole derivative compounds to come closer to the C-steel surface and the formed complex attracts the C-steel-charged surface and blocks the active centers of C-steel from reacting with HCl. These pathways suggest the formation a compact protected layer to

Table 9. Output Energies Were Calculated Using MCs for the Examined Two Pyrazole Derivatives in Gas and Simulated Liquid Phases on Fe (1 1 0)

compounds		E_T (kJ/mol)	E_{ads} (kJ/mol)	$E_{rig.}$ (kJ/mol)	$E_{def.}$ (kJ/mol)	$(dE_{ads}/dNi)(kJ/mol)$			
						inhibitors	H_3O^+	Cl^-	H_2O
gas	3	−262.90	−3479.73	−219.17	−3260.55				
	4	−273.75	−3501.31	−260.75	−3240.56				
liquid	3	−2389.36	−7655.26	−2399.88	−5255.38	−3507.37	−166.46	−128.57	−24.81
	4	−2359.77	−7636.41	−2400.94	−5235.47	−3541.44	−171.98	−122.46	−26.16
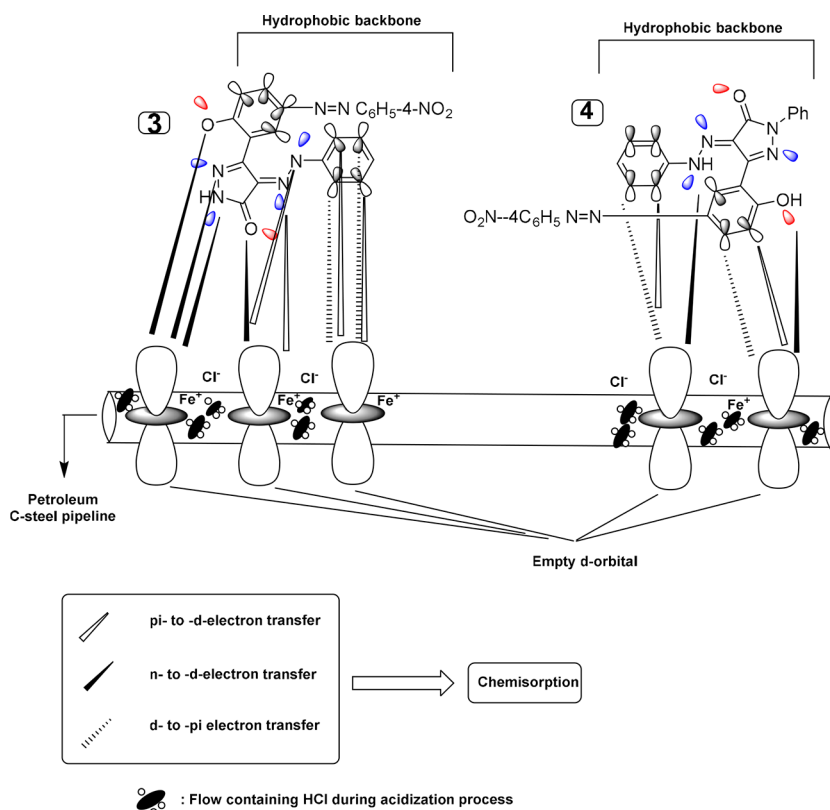
Figure 8. Expected adsorption scheme of the two synthesized pyrazole inhibitors on the C-steel surface.

shield the C-steel surface from the HCl contact. Electron sharing between the electron-rich function groups (aromatic and hetero-aromatic rings (pyrazolone, phenylhydrzenylidene, and phenyl-pyrazolone) in pyrazole compounds and the vacant 3d-orbital iron based on the donor-acceptor interaction concept forms a chemisorbed protective layer over the C-steel surface.[57] Figure 8 shows that this layer is a barrier against corrosion. The examined two synthesized pyrazoles exhibit excellent inhibition effectiveness due to: (i) their larger molecular size that may facilitate better surface coverage, (ii) the presence electron releasing groups (N and O atoms & π-bond in aryl group in compound 4), which promote the delocalized π-electrons on the active centers of the examined inhibitors.

3.7. Surface Analysis. AFM is an effective instrument for assessing how inhibitors affect the topography and surface roughness of metal surfaces in aggressive conditions. Figure 9 shows three-dimensional pictures of samples that were SiC-ground to 2000 grit and submerged in 1 M HCl for six hours at 25 °C before and after adding 500 M inhibitor 4. The C-steel's average roughness shows how its surface will interact with the environment. The creation of the protective oxide layer is reverted to by the least roughness (Ra = 2 nm) of polished C-

steel. Due to the production of porous corrosion products (iron chloride and oxide) over the surface of the C-steel, which is caused by the aggressive action of 1 M HCl, the surface roughness of the C-steel increased to 106 nm. The active centers of compound 4 (aromatic and hetero-aromatic rings (pyrazolone, phenylhydrzenylidene, and phenyl-pyrazolone), as well as halide and nitro groups), on the other hand, counteract the harmful effects of HCl by forming a protective film that adsorbed within the corrosion product layer, made it less porous, and protected the C-steel surface from the HCl effect. This effect is obvious from the lower C-steel roughness value (Ra = 44 nm).

3.8. Microbial-Induced Corrosion (MIC). The two synthesized pyrazole compounds (3 and 4) were investigated as antibacterial agents against potential MIC attacks on the growth rate of sulfate-reducing bacteria (SRB). Inhibitors 3 and 4 were put into the sealed growth medium vials at two different doses (15 and 30 ppm). The serial dilution strategy was used to create a series of various concentrations. After 21 days, the serially diluted sample vials with the injected inhibitors 3 and 4 are shown in Figure 10, along with the photographs taken of the incubated blank vials without inhibitors. The inhibitory activity of the examined compounds
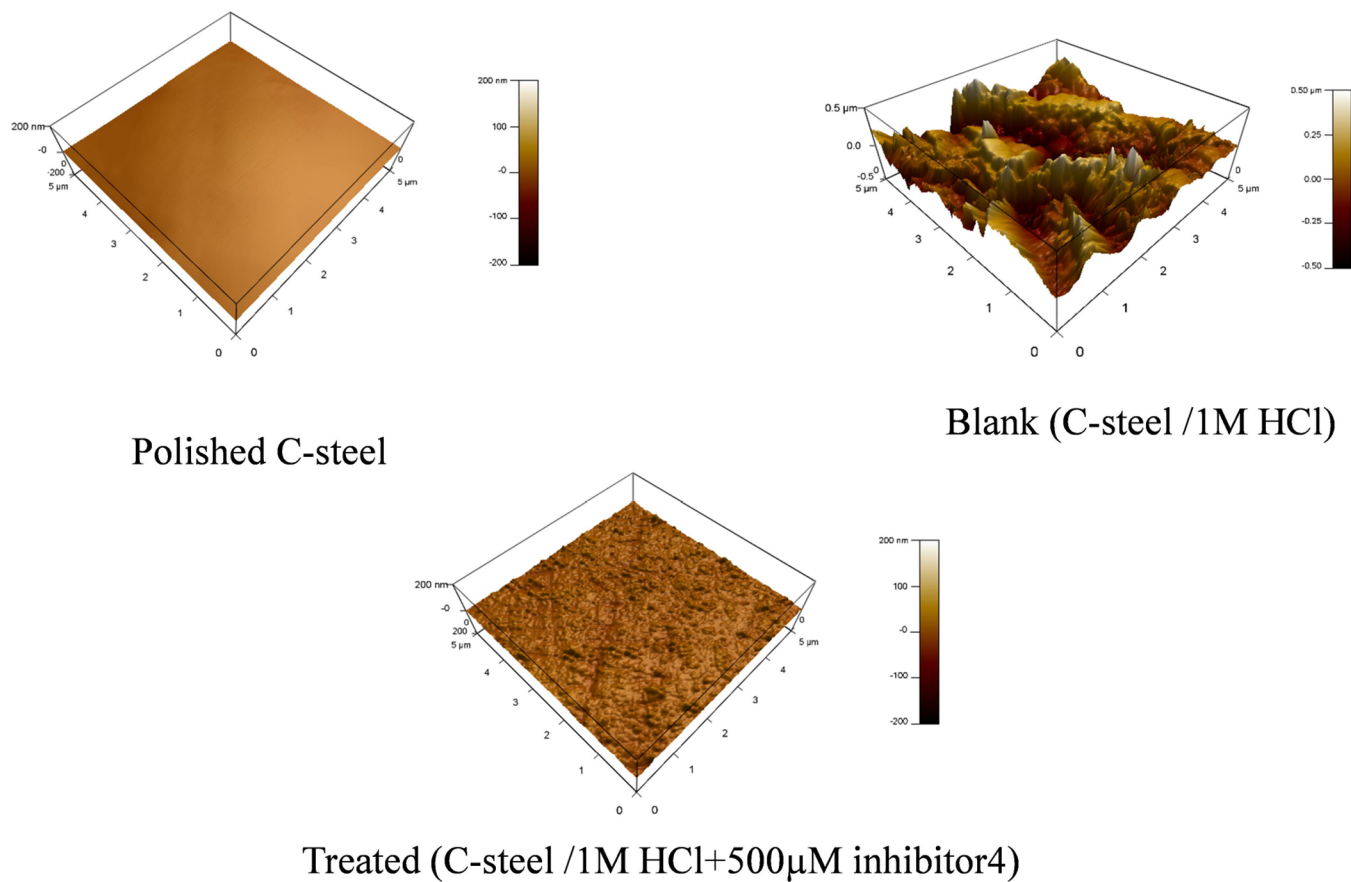
Figure 9. AFM images for the C-steel before and after immersion in treated and blank HCl.
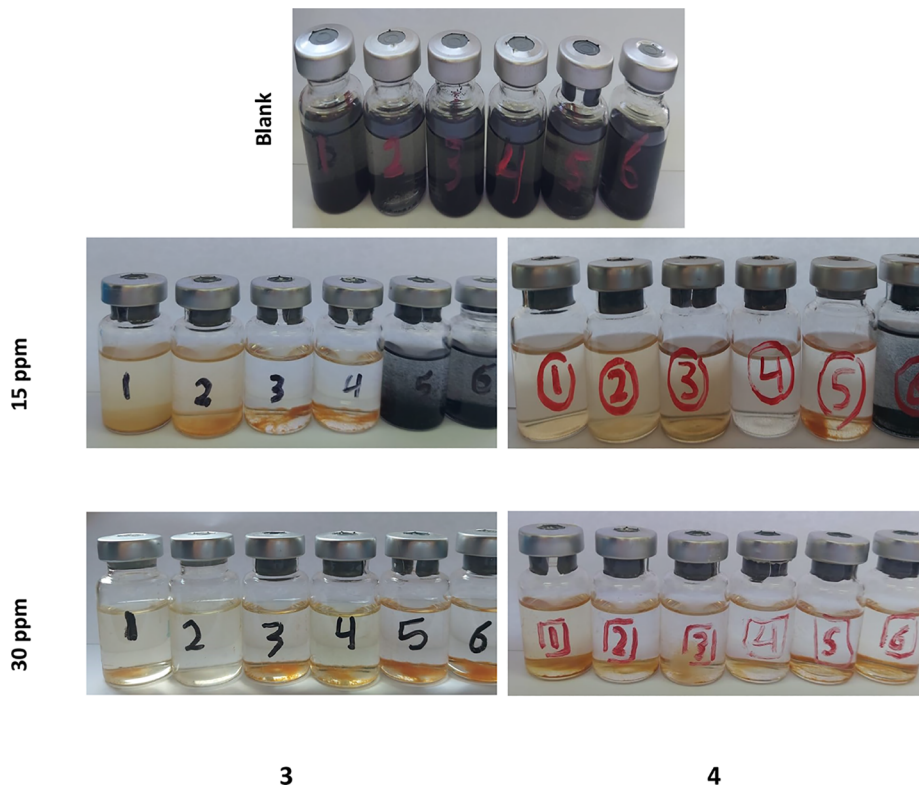

Figure 10. SRB growth quantification media kits injected with infected water samples with different concentrations of **3** and **4**.

was assessed by comparing the number of blackened vials (infected vials) to the blank. Significant biocidal activity has been observed in the tested substances. Since the observed bacterial count was 10^1 cells per milliliter at 15 ppm and 0 cells per milliliter at 30 ppm concentration, the predicted suppression effectiveness was up to 100% (Table 10).

Table 10. SRB Growth Bacterial Count for 3 and 4 at 40 °C for 21 Days

compounds	conc.	SRB count (cell/mL)	reduction in the SRB count (cell/mL)	efficiency (%)
blank		10^6		
3	15	10^4	10^2	66.7
	30	10^0	10^6	100
4	15	10^1	10^5	83.3
	30	10^0	10^6	100

4. CONCLUSIONS

1. The as-synthesized two pyrazole inhibitors were successfully prepared and acted as corrosion inhibitors for C-steel in 1 M HCl.
2. The tested inhibitors have good adsorption behavior on the C-steel due to the presence of effective groups that enhance the electron-donation process.
3. The adsorption of these pyrazole derivatives decreased the offensive action of 1 M HCl on the C-steel.
4. The change in E_{corr} of C-steel in HCl after pyrazole compounds was within the ±85 mV range, indicating the hybrid nature of these compounds.
5. The studied pyrazole **4** shifted the C-steel's I_{corr} and R_{ct} numeric values to 50.2 μA cm^{-2} and 295.4 Ω cm^2, respectively.
6. Compound **4** has a higher inhibition performance than compound **3** as it contains more active centers (benzene ring) that enforce the adsorption affinity.
7. Temperature enhanced the tested compounds' desorption; their IE % decreased, indicating their physical adsorption behavior at higher temperatures.
8. According to AFM analyses, surface roughness was considerably alleviated after adding 500 μ M of the corrosion inhibitor **4** to 1 M HCl. This confirmed the PP and EIS results.
9. E_{ads}. values obtained from MCs suggested the understudied compounds' spontaneous and strong adsorption inclination over the Fe alloy.
10. According to a preliminary analysis, the two synthetic pyrazole compounds displayed effective antibacterial properties against SRB.

ASSOCIATED CONTENT

Ⓢ Supporting Information

The Supporting Information is available free of charge at https://pubs.acs.org/doi/10.1021/acsomega.3c02333.

Synthesis of the inhibitors and spectroscopic characterizations, OCP, Bode and PP curves for C-steel in 1 M HCl, optimized molecular structures with electronic densities of the HOMO and LUMO and ESP map of the examined compounds' protonated form, and quantum chemical parameters of the examined protonated pyrazole derivatives (PDF)

AUTHOR INFORMATION

Corresponding Authors

Mahmoud M. Shaban − *Egyptian Petroleum Research Institute, 11727 Cairo, Egypt;* ⓞ orcid.org/0000-0002-7144-0316; Email: mahmoud_shaban26@yahoo.com

N. M. El Basiony − *Egyptian Petroleum Research Institute, 11727 Cairo, Egypt; School of Chemical Engineering, Sungkyunkwan University, Suwon 16419, South Korea;* Email: n.elbasiony@skku.edu

Emad E. El-Katori − *Chemistry Department, Faculty of Science, New Valley University, El-Kharga 72511, Egypt;* ⓞ orcid.org/0000-0001-9693-9546; Email: emad_992002@yahoo.com

Moaz M. Abdou − *Egyptian Petroleum Research Institute, 11727 Cairo, Egypt;* ⓞ orcid.org/0000-0003-0253-5714; Email: moaz.chem@gmail.com

Authors

A. Bahgat Radwan − *Center for Advanced Materials, Qatar University, Doha, Qatar;* ⓞ orcid.org/0000-0003-1115-3590

Ahmed Abu-Rayyan − *Faculty of Arts & Science, Applied Science Private University, Amman 11931, Jordan*

Nawal H. Bahtiti − *Faculty of Arts & Science, Applied Science Private University, Amman 11931, Jordan*

Complete contact information is available at: https://pubs.acs.org/10.1021/acsomega.3c02333

Notes

The authors declare no competing financial interest.

REFERENCES

(1) El-Katori, E. E.; El-Saeed, R. A.; Abdou, M. M. Anti-corrosion and antimicrobial evaluation of novel water-soluble bis azo pyrazole derivative for carbon steel pipelines in petroleum industries by experimental and theoretical studies. *Arab. J. Chem.* **2022**, *15*, No. 104373.

(2) El-Saeed, R. A.; Hosny, R.; Mubarak, M. F.; Abdou, M. M.; Shoueir, K. R. An innovative SiO2-pyrazole nanocomposite for Zn (II) and Cr (III) ions effective adsorption and anti-sulfate-reducing bacteria from the produced oilfield water. *Arab. J. Chem.* **2022**, *15*, No. 103949.

(3) Abbas, M. A.; Eid, A. M.; Abdou, M. M.; Elgendy, A.; El-Saeed, R. A.; Zaki, E. G. Multifunctional aspects of the synthesized pyrazoline derivatives for AP1 5L X60 steel protection against MIC and acidization: electrochemical, in silico, and SRB insights. *ACS Omega* **2021**, *6*, 8894−8907.

(4) Ashassi-Sorkhabi, H.; Ghasemi, Z.; Seifzadeh, D. The inhibition effect of some amino acids towards the corrosion of aluminum in 1 M HCl+ 1 M H₂SO₄ solution. *Appl. Surf. Sci.* **2005**, *249*, 408−418.

(5) Altwaiq, A.; Khouri, J.; Al-luaibi, S. S.; Lehmann, R.; Drücker, H.; Vogt, C. The role of extracted alkali lignin as corrosion inhibitor. *J. Mater. Environ. Sci.* **2011**, *2*, 259−270.

(6) Hosseini, M. G.; Ehteshamzadeh, M.; Shahrabi, T. Protection of mild steel corrosion with Schiff bases in 0.5 M H₂SO₄ solution. *Electrochim. Acta* **2007**, *52*, 3680−3685.

(7) Fan, H. B.; Fu, C. Y.; Wang, H. L.; Guo, X. P.; Zheng, J. S. Inhibition of corrosion of mild steel by sodium n, n-diethyl dithiocarbamate in hydrochloric acid solution. *Br. Corros. J.* **2002**, *37*, 122−125.

(8) Abdou, M. M.; El-Haddad, M. N. Synthesis of tolyl guanidine as copper corrosion inhibitor with a complementary study on electrochemical and in silico evaluation. *Sci. Rep.* **2022**, *12*, 14893.

(9) Yassin, A. Y.; Abdelghany, A. M.; Shaban, M. M.; Abdallah, Y. M. Synthesis, characterization and electrochemical behavior for API 5L X70 carbon steel in 5% sulfamic acid medium using PVVH/PEMA

blend filled with gold nanoparticles. *Colloids Surf. A: Physicochem. Eng. Asp.* **2022**, *635*, No. 128115.

(10) Hasanov, R.; Bilge, S.; Bilgiç, S.; Gece, G.; Kılıç, Z. Experimental and theoretical calculations on corrosion inhibition of steel in 1 M H_2SO_4 by crown type polyethers. *Corros. Sci.* **2010**, *52*, 984−990.

(11) Lgamri, A.; Abou El Makarim, H.; Guenbour, A.; Bachir, A. B.; Aries, L.; El Hajjaji, S. Electrochemical study of the corrosion behaviour of iron in presence of new inhibitor in 1 M HCl. *Progr. Org. Coat.* **2003**, *48*, 63−70.

(12) Abd El-Lateef, H. M.; Abdallah, Z. A.; Ahmed, M. S. M. Solvent-free synthesis and corrosion inhibition performance of Ethyl 2-(1, 2, 3, 6-tetrahydro-6-oxo-2-thioxopyrimi din-4-yl) ethanoate on carbon steel in pickling acids: Experimental, quantum chemical and Monte Carlo simulation studies. *J. Mol. Liq.* **2019**, *296*, 111800−111815.

(13) Abdou, M. M.; Seferoğlu, Z.; Fathy, M.; Akitsu, T.; Koketsu, M.; Kellow, R.; Amigues, E. Synthesis and chemical transformations of 3-acetyl-4-hydroxyquinolin-2 (1 H)-one and its N-substituted derivatives: bird's eye view. *Res. Chem. Intermed.* **2019**, *45*, 919−934.

(14) Abdou, M. M.; El-Saeed, R. A.; Abozeid, M. A.; Sadek, M. G.; Zaki, E.; Barakat, Y.; Ibrahim, H.; Fathy, M.; Shabana, S.; Amine, M. Advancements in tetronic acid chemistry. Part 1: Synthesis and reactions. *Arab. J. Chem.* **2019**, *12*, 464−475.

(15) Abdou, M. M. Chemistry of 4-hydroxy-2 (1H)-quinolone. Part 2. As synthons in heterocyclic synthesis. *Arab. J. Chem.* **2018**, *11*, 1061−1071.

(16) Abdou, M. M. Utility of 4-hydroxythiocoumarin in organic synthesis. *Arab. J. Chem.* **2017**, *10*, S3955−S3961.

(17) Abdou, M. M.; El-Saeed, R. A.; Elattar, K. M.; Seferoğlu, Z.; Boukouvalas, J. Advancements in tetronic acid chemistry. Part 2: use as a simple precursor to privileged heterocyclic motifs. *Molecular diversity. Mol. Diversity* **2016**, *20*, 989−999.

(18) Abdou, M. M.; El-Saeed, R. A.; Bondock, S. Recent advances in 4-hydroxycoumarin chemistry. Part 2: Scaffolds for heterocycle molecular diversity. *Arab. J. Chem.* **2019**, *12*, 974−1003.

(19) Abdou, M. M.; El-Saeed, R. A.; Bondock, S. Recent advances in 4-hydroxycoumarin chemistry. Part 1: Synthesis and reactions. *Arab. J. Chem.* **2019**, *12*, 88−121.

(20) El-Mahalawy, A. M.; Abdou, M. M.; Wassel, A. R. Physical and optoelectronic characteristics of novel low-cost synthesized coumarin dye-based metal-free thin films for light sensing applications. *Mater. Sci. Semicond. Process.* **2022**, *137*, No. 106225.

(21) Abdou, M. M.; Abu-Rayyan, A.; Bedir, A. G.; Abdel-Fattah, S.; Omar, A. M. A.; Ahmed, A. A.; El-Desoky, E. S. I.; Ghaith, E. A. 3-(Bromoacetyl) coumarins: unraveling their synthesis, chemistry, and applications. *RSC Adv.* **2021**, *11*, 38391−38433.

(22) El-Mahalawy, A. M.; Abdou, M. M.; Wassel, A. R. Structural, spectroscopic and electrical investigations of novel organic thin films bearing push-pull azo−Phenol dye for UV photodetection applications. *Spectrochim. Acta A* **2021**, *248*, No. 119243.

(23) Eid, A. M.; Shaaban, S.; Shalabi, K. Tetrazole-based organoselenium bi-functionalized corrosion inhibitors during oil well acidizing: Experimental, computational studies, and SRB bioassay. *J. Mol. Liq.* **2020**, *298*, No. 111980.

(24) Abousalem, A. S.; Ismail, M. A.; Fouda, A. S. A complementary experimental and in silico studies on the action of fluorophenyl-2, 2′-bichalcophenes as ecofriendly corrosion inhibitors and biocide agents. *J. Mol. Liq.* **2019**, *276*, 255−274.

(25) Wang, J.; Hou, B.; Xiang, J.; Chen, X.; Gu, T.; Liu, H. The performance and mechanism of bifunctional biocide sodium pyrithione against sulfate reducing bacteria in X80 carbon steel corrosion. *Corros. Sci.* **2019**, *150*, 296−308.

(26) Metwally, M. A.; Bondock, S.; El-Desouky, E. I.; Abdou, M. M. A facile synthesis and tautomeric structure of novel 4-arylhydrazono-3-(2-hydroxyphenyl)-2-pyrazolin-5-ones and their application as disperse dyes. *Color. Technol.* **2013**, *129*, 418−424.

(27) Abdou, M. M.; Bondock, S.; El-Desouky, S. I.; Metwally, M. A. Synthesis, spectroscopic studies and technical evaluation of novel disazo disperse dyes derived from 3-(2-hydroxyphenyl)-2-pyrazolin-5-ones for dyeing polyester fabrics. *Am. J. Chem.* **2013**, *3*, 59−67.

(28) Metwally, M. A.; Bondock, S. A.; El-Desouky, S. I.; Abdou, M. M. Synthesis, tautomeric structure, dyeing characteristics, and antimicrobial activity of novel 4-(2-arylazophenyl)-3-(2-hydroxyphenyl)-1-phenyl-2-pyrazolin-5-ones. *J. Korean Chem. Soc.* **2012**, *56*, 82−91.

(29) Metwally, M. A.; Bondock, S.; El-Desouky, S. I.; Abdou, M. M. Synthesis, Structure Investigation and Dyeing Assessment of Novel Bisazo Disperse Dyes Derived from 3-(2'-Hydroxyphenyl)-1-phenyl-2-pyrazolin-5-ones. *J. Korean Chem. Soc.* **2012**, *56*, 348−356.

(30) El Basiony, N. M.; Badr, E. E.; Baker, S. A.; El-Tabei, A. S. Experimental and theoretical (DFT&MC) studies for the adsorption of the synthesized Gemini cationic surfactant based on hydrazide moiety as X-65 steel acid corrosion inhibitor. *Appl. Surf. Sci.* **2021**, *539*, No. 148246.

(31) Fouda, A. S.; Al-Sarawy, A. A.; El-Katori, E. E. Pyrazolone derivatives as corrosion inhibitors for C-steel in hydrochloric acid solution. *Desalination* **2006**, *201*, 1−13.

(32) Migahed, M. A.; Azzam, E. M. S.; Morsy, S. M. I. Electrochemical behaviour of carbon steel in acid chloride solution in the presence of dodecyl cysteine hydrochloride self-assembled on gold nanoparticles. *Corros. Sci.* **2009**, *51*, 1636−1644.

(33) Khaled, K. F. New synthesized guanidine derivative as a green corrosion inhibitor for mild steel in acidic solutions. *Int. J. Electrochem. Sci.* **2008**, *3*, 462−475.

(34) Labjar, N.; Lebrini, M.; Bentiss, F.; Chihib, N. E.; El Hajjaji, S.; Jama, C. Corrosion inhibition of carbon steel and antibacterial properties of aminotris-(methylenephosphonic) acid. *Mater. Chem. Phys.* **2010**, *119*, 330−336.

(35) Bentiss, F.; Outirite, M.; Traisnel, M.; Vezin, H.; Lagrenée, M.; Hammouti, B.; Al-Deyab, S. S.; Jama, C. Improvement of corrosion resistance of carbon steel in hydrochloric acid medium by 3, 6-bis (3-pyridyl) pyridazine. *Int. J. Electrochem. Sci.* **2012**, *7*, 1699−1723.

(36) Hegazy, M. A.; Badawi, A. M.; Abd El Rehim, S. S.; Kamel, W. M. Corrosion inhibition of carbon steel using novel N-(2-(2-mercaptoacetoxy) ethyl)-N, N-dimethyl dodecan-1-aminium bromide during acid pickling. *Corros. Sci.* **2013**, *69*, 110−122.

(37) Szklarska-Smiaiowska, Z. *Electrochemical and optical techniques for the study of metallic corrosion*; Kluwer Academic: the Netherlands, 1991; Vol. *203*, pp. 545 −570.

(38) Langmuir, I. The constitution and fundamental properties of solids and liquids. II. Liquids. *J. Am. Chem. Soc.* **1917**, *39*, 1848−1906.

(39) Kaminski, M.; Szklarska-Smialowska, Z. Adsorption of thiophene derivatives on steel in sulphuric acid solutions. *Corros. Sci.* **1973**, *13*, 557−565.

(40) Putilova, I. N.; Balezin, S. A., Barannik, V. P. *Metallic Corrosion Inhibitors*; Pergamon Press, 1961.

(41) Quartarone, G.; Battilana, M.; Bonaldo, L.; Tortato, T. Investigation of the inhibition effect of indole-3-carboxylic acid on the copper corrosion in 0 5 M H2SO4. *Corros. Sci.* **2008**, *50*, 3467−3474.

(42) Behpour, M.; Ghoreishi, S. M.; Soltani, N.; Salavati-Niasari, M.; Hamadanian, M.; Gandomi, A. Electrochemical and theoretical investigation on the corrosion inhibition of mild steel by thiosalicylaldehyde derivatives in hydrochloric acid solution. *Corros. Sci.* **2008**, *50*, 2172−2181.

(43) Eddy, N. O.; Ita, B. I.; Ibisi, N. E.; Ebenso, E. E. Experimental and quantum chemical studies on the corrosion inhibition potentials of 2-(2-oxoindolin-3-ylideneamino) acetic acid and indoline-2, 3-dione. *Int. J. Electrochem. Sci.* **2011**, *6*, 1027−1044.

(44) Issa, R. M.; Awad, M. K.; Atlam, F. M. Quantum chemical studies on the inhibition of corrosion of copper surface by substituted uracils. *Appl. Surf. Sci.* **2008**, *255*, 2433−2441.

(45) Öğretir, C.; Mihci, B.; Bereket, G. Quantum chemical studies of some pyridine derivatives as corrosion inhibitors. *J. Mol. Struct.* **1999**, *488*, 223−231.

(46) Musa, A. Y.; Mohamad, A. B.; Kadhum, A. A. H.; Takriff, M. S. Synergistic effect of potassium iodide with phthalazone on the

corrosion inhibition of mild steel in 1.0 M HCl. *Corros. Sci.* **2011**, *53*, 3672−3677.

(47) Obi-Egbedi, N. O.; Obot, I. B.; El-Khaiary, M. I.; Umoren, S. A.; Ebenso, E. E. Computational simulation and statistical analysis on the relationship between corrosion inhibition efficiency and molecular structure of some phenanthroline derivatives on mild steel surface. *Int. J. Electrochem. Sci.* **2011**, *6*, 5649−5675.

(48) Elaraby, A.; Elgendy, A.; Abd-El-Raouf, M.; Migahed, M. A.; El-Tabei, A. S.; Abdullah, A. M.; Al-Qahtani, N. H.; Alharbi, S. M.; Shaban, S. M.; Kim, D. H.; El Basiony, N. M. Synthesis of Gemini cationic surfactants based on natural nicotinic acid and evaluation of their inhibition performance at C-steel/1 M HCl interface: electrochemical and computational investigations. *Colloids Surf.* **2023**, *659*, No. 130687.

(49) Udhayakala, P.; Rajendiran, T. V. A theoretical evaluation on benzothiazole derivatives as corrosion inhibitors on mild steel. *Der Pharma Chem.* **2015**, *7*, 92−99.

(50) El-Tabei, A. S.; Hegazy, M. A.; Bedair, A. H.; El Basiony, N.; Sadeq, M. A. Experimental and theoretical (DFT&MC) studies for newly synthesized cationic amphiphilic substance based on a naphthol moiety as corrosion inhibitor for carbon steel during the pickling process. *J. Mol. Liq.* **2021**, *331*, No. 115692.

(51) Ashassi-Sorkhabi, H.; Shaabani, B.; Seifzadeh, D. Effect of some pyrimidinic Shciff bases on the corrosion of mild steel in hydrochloric acid solution. *Electrochim. Acta* **2005**, *50*, 3446−3452.

(52) Bentiss, F.; Traisnel, M.; Gengembre, L.; Lagrenée, M. Inhibition of acidic corrosion of mild steel by 3, 5-diphenyl-4H-1, 2, 4-triazole. *Appl. Surf. Sci.* **2000**, *161*, 194−202.

(53) Prabhu, R. A.; Venkatesha, T. V.; Shanbhag, A. V.; Kulkarni, G. M.; Kalkhambkar, R. G. Inhibition effects of some Schiff's bases on the corrosion of mild steel in hydrochloric acid solution. *Corros. Sci.* **2008**, *50*, 3356−3362.

(54) Annand, R. R.; Hurd, R. M.; Hackerman, N. Adsorption of monomeric and polymeric amino corrosion inhibitors on steel. *J. Electrochem. Soc.* **1965**, *112*, 138.

(55) Cook, E. L.; Hackerman, N. Adsorption of polar organic compounds on steel. *J. Phys. Chem.* **1951**, *55*, 549−557.

(56) Aljourani, J.; Golozar, M. A.; Raeissi, K. The inhibition of carbon steel corrosion in hydrochloric and sulfuric acid media using some benzimidazole derivatives. *Mater. Chem. Phys.* **2010**, *121*, 320−325.

(57) Sastri, V. S.; Perumareddi, J. R. Molecular orbital theoretical studies of some organic corrosion inhibitors. *Corrosion* **1997**, *53*, 617.